Revealing the heterogeneous nucleation behavior of equiaxed grains of inoculated Al alloys during directional solidification

Yijiang Xu[1], Daniele Casari[2], Ragnvald H. Mathiesen[2], Yanjun Li[1*]

[1] Department of Materials Science and Engineering, Norwegian University of Science and Technology (NTNU), N-7491 Trondheim, Norway

[2] Department of Physics, Norwegian University of Science and Technology (NTNU), N-7491 Trondheim, Norway

*Corresponding author: E-mail address: yanjun.li@ntnu.no

Abstract

An in-situ study on the directional solidification of an inoculated Al-20 wt%Cu alloy under well-controlled constant cooling rates and temperature gradients has been carried out using a microfocus X-radiography set-up. The influences of temperature gradient and cooling rate on the heterogeneous nucleation rate and growth kinetics of equiaxed grains have been studied quantitatively. It is shown that under the same cooling rate, the nucleation rate of grains decreases with increasing temperature gradient. A high temperature gradient also promotes preferential growth of dendrite arms along the temperature gradient direction, and therefore the formation of elongated grains. However, the temperature gradient effects on nucleation and grain growth decrease with increasing cooling rate. It is revealed that the propagation velocity of the nucleation front in directional solidification castings is approximately equal to the ratio between cooling rate $\dot{T}$ and temperature gradient G. Based on the experimental observations, a novel numerical grain size prediction model has been proposed, in which the temperature gradient effect on the nucleation kinetics was rigorously treated by introducing two new concepts termed as 'inhibited nucleation zone'(INZ) and 'active nucleation zone'(ANZ). The model has been applied to simulate the present in-situ solidification experiments. A good agreement was achieved between the predicted grain number density and the experimental measurements, showing the importance of including the temperature gradient effect on heterogeneous nucleation. Furthermore, the present model also has the capability to predict the temperature gradient necessary for the transition from equiaxed to columnar grain growth.

Key words: Heterogeneous nucleation, Grain growth, Directional solidification, Grain refinement, Al alloys

1. Introduction

Grain refinement by inoculation is an important technique to reduce hot tearing susceptibility and to improve the structure homogeneity and mechanical properties of aluminum castings [1-4]. The grain refinement mechanism by inoculation and the influences of different factors on the grain refinement performance have been extensively studied in the last decades. Now it has been well accepted that the heterogeneous nucleation of grains on inoculant particles is a deterministic, instead of stochastic process, while the undercooling needed for the formation of a freely growing grain is dependent on the size of inoculant particles [5-9]. In addition to the type, size distribution and addition amount of inoculant particles, the chemical composition of alloys also strongly influences the grain refinement effect, which stems from the solute effect on restricting grain growth. The growth restriction effect can be evaluated by the so-called Q factors of alloying elements in the alloys [5, 10]. Generally, a high Q value is beneficial for the grain refinement, provided that the solute does not interact with the inoculant particles or other solutes. Also, a nucleation stopping mechanism is important for understanding the grain refinement behavior of inoculated aluminum alloys. Recalescence has long been understood to be the effective nucleation stopping mechanism for most of the castings where recalescence is non-negligible [5, 11]. For those castings where recalescence is not present, for example, unidirectional solidification, it has been proven, both experimentally and by numerical modeling, that the nucleation stops due to solute segregation stifling [12].

So far most of the experimental studies on grain refinement have been based on TP-1 type test [5, 13-18], which can provide standard solidification conditions for different inoculated alloys. The experimental results of TP-1 test have been widely used to validate the grain size prediction models, most of which have been based on the isothermal melt solidification assumption. However, temperature gradients always exist in the melt of castings. This is also true for TP-1 type castings, although the temperature gradient in the melt is small.

The effect of temperature gradient on the columnar to equiaxed transition (CET) has been extensively studied by both well controlled unidirectional solidification experiments in Bridgman furnace and non-steady state directional solidification by chill

casting methods [19-24], as well as modeling studies [25-31]. It is well understood that a lower temperature gradient in the melt promotes CET.

Research efforts have also been made to understand the effects of addition level of grain refiners [32] and solidification velocity (or pulling velocity) [23, 32-34] on the grain size of inoculated aluminum alloys during Bridgman type directional solidification. These studies show that a higher solidification velocity favors the formation of smaller and more equiaxed grains. However, dedicated studies on the effect of temperature gradient on the nucleation and growth behavior of equiaxed grains in inoculated aluminum alloys have been few, and the conclusions are somewhat contradictory and confusing. Jung et al. [23] studied the equiaxed grain size of Al-5Ti-1B inoculated Al-Ni alloys under two different temperature gradients (G=14 K/cm and G=20 K/cm) by Bridgman-type directional solidification experiments. The experimental results show that the grain size is smaller for the high G condition than the low G condition within the whole pulling velocity range (even under the same cooling rate for the two different G conditions). Vandyoussefi et al. [32] investigated the effects of varying G on the grain structure and size in Bridgman solidification samples of inoculated Al-4.15 wt.% Mg alloy by both experiments and cellular automaton-finite element (CA-FE) modeling. It showed that 'the grains are relatively large and equiaxed at low G, and become smaller and progressively more elongated as G is increased' at constant pulling velocity [32]. Since at constant pulling velocity, a change of G will also change the cooling rate of the melt, the size and morphology evolution of the equiaxed grains is a result of the combined effect of G and cooling rate. Thus, it is difficult to isolate the G effect on the nucleation of grains. Based on the analytical analysis using the interdependence model [35], Easton et al. [3] suggested that an increase in temperature gradient has two effects on the grain size. One is to decrease the grain size by decreasing the distance from the growing grain to the point of maximum supercooling. The other is to reduce the magnitude of the supercooling, which would increase the grain size and in extreme cases suppress equiaxed nucleation entirely. It was also suggested that high temperature gradient is "more influential at much higher cooling rates" for grain refinement.

To understand the heterogeneous nucleation and grain growth behavior, and to predict the grain size in castings of inoculated aluminum alloys, many numerical and analytical models have been developed in the last decades [5, 11, 12, 36-47]. The early models [5, 11, 37, 43, 44, 47] are mostly based on the spatially isothermal melt assumption and

recalescence nucleation-stifling mechanism, following the framework of Maxwell-Hellawell model [11].

Quested and Greer [40] proposed a soft impingement induced nucleation stopping mechanism, which can be used for grain size prediction of steady-state directional solidification cases without recalescence. In their model [40], the thickness of the soft impingement zone, where no new nucleation could happen due to reduced undercooling, was assumed as twice the radius of growing grain, $2R$ for spherical grains, and as the radius of growing grain, R, for dendritic grains. Such a soft impingement zone was later also considered by Shu et al. [44] as the 'solute suppressed nucleation' zone and StJohn et al. as the 'nucleation free zone' [45]. In a recent work, Du and Li [46] did a more rigorous treatment of the thickness of the solute diffusion layer and the soft impingement zone around growing grains, and proposed a new grain size prediction model based on the solute segregation stifling nucleation mechanism, applicable for solidification cases without recalescence. After a further development to include the dendritic growth kinetics of grains, the model has been validated by the in-situ isothermal melt solidification experiments with constant cooling rate [12]. Though intended for directional solidification, the above models are still based on a local isothermal melt solidification assumption, while the effects of temperature gradient on the heterogeneous nucleation of equiaxed grains are neglected.

There have been some modeling works that consider the temperature gradient indirectly. Vandyoussefi et al. [32], Quested et al. [18, 48] and Liu et al. [49] used the cellular automaton-finite element (CA-FE) method to model the grain refinement of Al alloys during Bridgman-type directional solidification. By using a Gaussian distribution of nucleation events as a function of undercooling [50, 51], the above models are able to illustrate the trends in the variation of grain size with pulling velocity and temperature gradient (only one simulation test by Vandyoussefi et al. [32]). However, as commented by Quested [18], heterogeneous nucleation is not treated as deterministic. Besides CA-FE, several multiscale modeling approaches were developed to simulate the as-cast grain size distribution of real castings, in which nucleation is treated based on the free growth criterion [5] (critical nucleation undercooling determined by the nucleant size). Bottger et al. [41] coupled the microscopic phase filed model with a 1D temperature solver. Mirihanage and Browne [52] used a combined analytical/numerical 2D model to model the nucleation and growth of equiaxed grains during ingot casting. Bedel et al.

[53] did the process-scale modeling of DC-casting. Nevertheless, there is still a way to go, and more rigorous treatment of grain nucleation on inoculant particles under temperature gradients is still in demand.

In this work, a series of in-situ X-radiography solidification experiments have been designed and carried out to investigate the isolated effect of temperature gradient and cooling rate on the heterogeneous nucleation and grain growth of inoculated Al alloys during directional solidification. Based on the experimental findings, a novel grain size prediction model which includes the effect of the temperature gradient on heterogeneous nucleation is proposed. The modeling results have also been compared with the experimental results.

2. Experimental

The material used in the experimental study is an Al-20Cu (wt.%) alloy prepared by melting 5N (99.999%) purity aluminum and 4N (99.99%) purity copper in a clay graphite crucible using a Nabertherm melting furnace. After complete melting and mixing of the raw metals, 0.05 wt.% Al-5Ti-1B (wt.%) master alloy (of the total melt) was added, followed by stirring and 30 minutes holding. Afterwards, the melt was cast into a rectangular copper mold and solidified into a small ingot. Plate-shaped samples of roughly 1 mm thickness were cut from the ingot, manually ground and polished, up to 1 μm silica suspension, to reach the final dimension of 5 × 50 × 0.2 ±0.01 mm (X×Y×Z).

The microfocus X-radiography setup used in the current study, including the XRMON Gradient Furnace, has been extensively described elsewhere [54-56]. In the present study, a Mo transmission target with fine focus power setting of 50 keV and 60 μA was employed for the X-ray source. The sample was aligned in a configuration where the broad surface (X-Y plane) of the sheet-like sample is perpendicular to the gravity (Z || g), by which the melt convection and grain motion were reduced to a large extent. The Bridgman furnace was operated in the so-called near-isothermal mode [12, 57], and later in standard directional solidification mode with imposed temperature gradients G along the sample length direction (G || Y). In the near-isothermal mode, the furnace temperature (melt temperature) at the commencement of the experiment is 630 ^{o}C; During directional solidification experiments, the starting temperature of the liquid in the cold side of the furnace was set as 630 ^{o}C, while the temperature in the hot side

was set to the designated ones based on the temperature gradient G_Y, e.g., the furnace/melt temperature at the hot side is 730 °C with G_Y =10 K/mm prior to solidification. Constant cooling rates $\dot{T}$, in the range of 0.025-1.0 K/s, were applied by a controlled power down technique, rather than by sample motion. Due to the efficient heat conduction, the latent heat released in the thin sample during solidification could be quickly extracted through the glassy carbon crucible and the sample holder with large heat capacity and therefore constant cooling rates can be achieved [12]. The size of the field of view (FOV) in the settings applied was 2877x1916 μm^2. The images were recorded at a frame rate of 2 Hz. The images were subsequently processed with ImageJ [58] to enhance the contrast, and extract microstructure information.

3. Experimental Results

3.1. Effect of temperature gradient

3.1.1. Solidification at cooling rate of 0.025 K/s

Selected representative images from the X-radiography sequences recorded in-situ during solidification of inoculated Al-20Cu at constant cooling rate of 0.025 K/s, are shown in Fig. 1. The time labeled in the images indicates the solidification time since the first grain was observed in the FOV (t=0 for the first solidification event). The images in the left column are for near-isothermal condition with $G_Y \cong 0$, and the right column for the directional solidification with $G_Y = 5$ K/mm.

It has to be noted that for the near-isothermal melt solidification condition, a small temperature gradient ~0.2 K/mm exists in the melt along the X-axis indicated in Fig. 1, due to limitations in the present gradient furnace, which only allows for regulating *G* along the Y-axis [12]. Therefore, equiaxed grains appear slightly earlier in the right side of the FOV. However, in the Y-direction, parallel to the controlled heat extraction, no distinct temperature gradient exists, as evidenced by a rather symmetric grain nucleation at the upper side and lower side of the image. The small temperature gradient in the X-axis will not affect the generality for the comparison of the nucleation behavior in the Y-direction.

Under a temperature gradient of 5 K/mm (Fig. 1b), nucleation of grains (e.g., Grain A) starts from the cold side of the sample (upper side of the image), and gradually moves towards the hot side, along positive Y. It can be seen that the morphology of new grains

nucleated in the FOV is equiaxed in the initial growth stage, while it tends to become elongated as growth continues. Dendrite arms with tips pointing towards higher temperature, grow faster than the other dendrites. For example, in Grain B the dendrite arm 1, most likely along one of the <100> directions, grows faster than the other primary dendrite arms. In contrast, the growth of dendrite arms with tips pointing to lower temperature direction (dendrite arm 2 of Grain B) is very slow and therefore the dendrites have little development in the negative temperature gradient direction. This should be ascribed to the soft impingement of the solute segregation zone with that of the previously formed grains [59], for example, Grain A and Grain C. However, for those dendrite tips pointing to the positive Y direction, the dendrite growth can last for a long time until they are stopped by the newly formed grains, for example, dendrite arm 1 of Grain A. As a result, many grains have elongated, instead of equiaxed, morphology.

Another difference between the near-isothermal melt solidification and directional solidification is that the total grain number in the latter case is much smaller. The evolution of the total number of aluminum grains in the FOV as a function of solidification time since the turning up of the first grain has been extracted from the recorded X-radiographic images and plotted in Fig. 2. As can be seen from Fig. 1 and 2, in both solidification cases, the number of grains in the FOV increases with the solidification time, i.e., decreasing melt temperature, until a maximum value is reached and then remains constant. In near-isothermal solidification, a maximum number of 17 equiaxed grains is achieved in the FOV within 65 s, corresponding to an average nucleation rate of $2.37 \times 10^{8} m^{-3} s^{-1}$. However, in directional solidification, it takes 300 s to form only 9 grains in the whole FOV. The average nucleation rate is $2.64 \times 10^{7} m^{-3} s^{-1}$, which is about one order of magnitude smaller than that in near-isothermal solidification. The results show that the nucleation rate and the final grain number is reduced significantly when a temperature gradient is applied in the sample, although the cooling rate during the solidification process is the same.

The growth of primary dendrite arms of individual grains in these two solidification conditions has been analyzed through tracking the primary arm tips over time in the X-radiographic images. Each dendrite arm is labeled with a numbers 1 or 2 for grains A ~ F, as illustrated in Fig. 1. The primary dendrite arm length is measured from the nucleation center of grains, and the results are plotted in Fig. 3a. As can be seen, during

near-isothermal melt solidification, the difference in length of different primary dendrite arms in the same grain is quite small, showing an equiaxed growth. In contrast, at G = 5 K/mm, the length of different primary dendrite arms of each grain is very different; those dendrite arms with growth direction close to the positive temperature gradient direction grow much longer into the liquid.

The growth velocity of individual primary dendrite arms has been obtained from the first derivative of growth curves in Fig. 3a and the corresponding results are shown in Fig. 3b. As can be seen, during near-isothermal melt solidification, the growth velocity of different primary dendrite arms shows about the same behavior: the dendrite tip velocity reaches a peak value within 50 s, drops down sharply and then decreases gradually with increasing solidification time. In the late stage of grain growth, the tip velocity is very small, mostly in the range of 0.2~0.5μm/s, which should be ascribed to the constraining effect caused by the soft impingement of the solute diffusion filed. During directional solidification, a fast increase of growth velocity to the maximum followed by a sharp drop is also observed in the early stage of grain growth for those slow-growing dendrite arms, e.g., dendrite arm 2 of Grain B. The maximum growth velocity measured is about 3.5-4 μm/s, which is quite close to the ones in near-isothermal solidification (3.5-4.5 μm/s). However, for the fast-growing dendrites arms, the high growth velocity can keep for a much longer time (dendrite arm 1 of Grain A), until new grains nucleate and grow in front of the dendrite tip and therefore cause soft impingement. The reason that the dendrite arm could keep a high growth velocity for a longer time should be the lack of nucleation of new grains in front of the dendrite tip. As a consequence of such type of preferential growth of dendrite arms, a large fraction of elongated grains can be observed in the FOV of directional solidification.

The volume fraction of solid grains, f_s, as a function of solidification time is extracted from the in-situ solidification images under both near-isothermal melt and directional solidification conditions, as shown in Fig. 4. In the early stage of solidification during near-isothermal melt solidification, f_s increases much faster than that during directional solidification. After the nucleation process is completed (within the FOV) for both near-isothermal and directional solidification, the growth rate of f_s becomes similar for the two cases. It indicates that the evolution of f_s is controlled by both heterogeneous nucleation and grain growth. In the nucleation stage, the increase of f_s is slower, and dominated by the nucleation rate, which depends on the local undercooling and the

inoculant particles (number and size/potency). For directional solidification, nucleation rate, grain growth velocity and solidification front are influenced by the temperature gradient (thermal state of the sample), thus f_s delays in comparison to the near-isothermal melt solidification. While after nucleation has ceased, f_s is determined by grain growth and increases faster, which is similar for both solidification cases.

3.1.2. Solidification at cooling rate of 0.1 K/s

Fig. 5 shows the X-radiographic images taken during the solidification at a cooling rate of 0.1 K/s, with three different temperature gradients (G=0, 5, 10 K/mm). In comparison to the solidification cases of 0.025 K/s cooling rate shown in Fig. 1, the total number of grains formed in the FOV for the directional solidification condition with the same temperature gradient, G =5 K/s is much higher, showing that high cooling rate has the influence of promoting the nucleation of grains during directional solidification, which is the same trend as found for the near-isothermal melt solidification condition. By comparing the G =5 K/mm and G =10 K/mm conditions, one can find that for the latter condition, the total number of grains is less and that the grains become more elongated. Besides, the grain nucleation front of the directional solidification castings, as labeled by the dashed lines in Fig. 5b and 5c, propagates gradually towards the hot side of the FOV. The new grains formed in the nucleation front have the influence of blocking the growth of previously formed grains behind them by solutal impingement. For grains without new grains forming ahead of them, the grain growth is free to continue, and accordingly these grains will develop into elongated morphologies, e.g., Grain A and Grain B in Fig. 5c, or in the extreme case even into columnar dendrites if enough space is left free for propagation. The position of the nucleation front along the Y-direction, as a function of solidification time, was measured from the X-radiographic image sequences by ImageJ [58], and the results are plotted in Fig. 6a. Based on a linear fit to the experimental data, an average velocity of 20.2 and 11.9 μm/s was obtained for the propagation of the nucleation front under temperature gradients G=5 and 10 K/mm, respectively. These two values are very close to the moving velocity of liquidus temperature isotherm of the melt, calculated by $v = \dot{T}/G$, in the two directional solidification cases, 20 and 10 μm/s, respectively. It indicates that the propagation velocity of the nucleation front is proportional to the cooling rate while inversely proportional to the temperature gradient G.

The corresponding evolution of number of grains in the FOV as a function of solidification time is shown in Fig. 6b. As can be seen, both the nucleation rate and the final grain number density decrease with increasing temperature gradient. Different from the continuous growth curve of grain number with increasing solidification time during near-isothermal melt solidification, the evolution of grain number of directional solidification, especially at G = 10 K/s, shows a stepwise curve. This is consistent with the observed stepwise propagation character of grain nucleation front.

The grain growth in three different solidification cases at 0.1 K/s are also analyzed (not shown here). Growth behavior of dendrite arms similar to that for 0.025 K/s cooling rate (Fig. 3) is observed.

3.1.3. Solidification at cooling rate of 0.5 K/s

Fig. 7 shows the X-radiographic images recorded before and after nucleation ceasing in the melt of FOV solidified at 0.5 K/s cooling rate under different temperature gradients (G_Y =0, 5, 10, 15 K/mm). As can be seen, the total number of grains in the FOV decreases while the fraction of elongated grains increases with increasing temperature gradient, showing that a high G favors the preferential dendrite growth of grains and suppresses the nucleation of grains.

Fig. 8a shows the Y-position of the nucleation front as a function of solidification time. Again, the measured data points can be well fitted by a linear function, the slope of which indicates the propagation velocity of the nucleation front. For G=5, 10 and 15 K/mm, the nucleation front velocities are 98.5, 60.1 and 41.2 μm/s, respectively, close to $\dot{T}/G$ for each solidification condition.

The evolution of total grain number in the FOV with solidification time is shown in Fig. 8b. As can be seen, for all solidification cases the number of grains increase nearly linearly with time until nucleation stops in the FOV. It means that the number of grains nucleated per volume under constant $\dot{T}$ and G is uniform in the sample. It can also be seen that the grain nucleation velocity and the final grain number decrease with increasing temperature gradient. It further confirms that a higher temperature gradient has the influence of reducing the grain refinement efficiency of inoculant particles.

3.2. Effect of cooling rate

To further study the influence of cooling rate on the heterogeneous nucleation during directional solidification, different $\dot{T}$ values were applied under a fixed temperature gradient of G=5 K/mm, which is a typical temperature gradient during solidification of DC castings of aluminum ingots [60]. Fig. 9a displays the final grain number density after nucleation ceasing of in-situ samples, in comparison to the near-isothermal melt solidification samples under the same cooling rates. The final grain number densities were calculated by dividing the number of grains nucleated in the FOV by the total volume of the FOV (sample thickness=200 μm) directly. As can be seen, the final number density of grains increases as cooling rate increases in both solidification conditions. Present results agree well with the pulling-type directional solidification [33, 34] (controlling pulling velocity instead of cooling rate). It can also be seen that near-isothermal melt solidification samples always have higher grain number density than directional solidification samples at the same cooling rate. However, the difference in grain number density between the two solidification conditions decreases with increasing cooling rate. At the cooling rate of 1.0 K/s, the difference is already rather small. It means that a higher cooling rate can compensate the suppressing effect of temperature gradient on the heterogeneous nucleation of grains of inoculated aluminum alloys.

The average propagation velocity of the nucleation front under different cooling rates is shown in Fig. 9b. The propagation velocity was determined from the in-situ images using the same approach as used to extract the data shown in Fig. 6a and Fig. 8a. As can be seen, the propagation velocity increases with increasing cooling rate. Further, the experimental data are well fitted by a linear function with a slope equals to 198.6 μm/K, which is very close to the value of 1/G (200 μm/K). It further confirms that the average propagation velocity of the nucleation front is proportional to the cooling rate.

4. Model description

The numerical model used in this work is an extension to our previous isothermal melt solidification model [12], now modified to include the effect of temperature gradient. In the model, a specific calculation domain is defined, with a size of $2 \times 2 \times 2\ mm^3$, as shown in Fig. 10. In isothermal melt solidification, the solidification process starts from the nucleation of the first class of grains on the biggest inoculant particles in the whole melt. In directional solidification, on the contrary, solidification starts from the

cold side of the melt, and only a fraction of the most potent particles (with larger size and therefore smaller free growth undercooling) in the left side of the calculation domain can be activated to nucleate grains in the beginning. Afterwards, the nucleation of new grains in the melt with temperature lower than the critical nucleation temperature can be calculated in real time (see detailed description in Section 4.1) with a movement of the liquids isothermal line. The propagation velocity of liquidus isotherm is $\dot{T}/G$. Hetrogeneous nucleation of grains proceeds progressively from the cold side to the hot side of the melt, as observed from the in-situ X-radiography experiments.

4.1. Nucleation

The heterogeneous nucleation of grains on inoculant particles is based on the free growth criterion [5]. The quasi-steady state solute concentration profile in the liquid outside of the spherical grain envelope can be approximated as [61, 62]:

$$C_l(r) = C_0 + \frac{R_g}{r}(C_l^* - C_0) \tag{1}$$

where C_0 is the bulk melt composition, C_l^* the solute concentration in the liquid at the solid/liquid interface, R_g the radius of grain envelope, and r the distance to the center of the grain.

Fig. 11a is a schematic drawing to show the liquidus temperature profile of the liquid metal around a growing equiaxed grain, with a temperature gradient G_Y, and the corresponding supercoolings. As shown, in the direction perpendicular to the temperature gradient no temperature gradient exists; the nucleation of grains on inoculant particles is the same as the isothermal melt solidification condition. Due to the reduced supercooling by solute segregation, nucleation of new grains in the melt within the solute suppressed nucleation (SSN) zone is completely inhibited. The thickness of the 'inhibited nucleation zone' (INZ), δ_{INZ-I}, is the same as that of the solute suppressed nucleation zone δ_{SSN} (shown in Fig. 11b), given by [12, 46]:

$$\delta_{INZ-I,}(\theta = \frac{\pi}{2}) = \delta_{SSN} = \left(\frac{\Delta T - \Delta T_r}{\Delta T - \Delta T_{fg}}\right) \cdot R_g \tag{2}$$

where ΔT, ΔT_r and ΔT_{fg} are the maximum total undercooling in the melt (when the temperature gradient is not considered), curvature undercooling and free growth undercooling for specific inoculation particles under consideration, respectively.

In the other directions, the undercooling of the melt is influenced not only by the solute concentration but also by the temperature gradient. Thus, the INZ is obviously different from the SSN zone, and it is a function of the angle θ between the direction under consideration and the temperature gradient. Along G_Y, the thickness of the INZ has two extreme values. Towards the higher temperature side ($\theta = 0$), INZ includes two parts. One part is within the solute segregation zone, caused by both the segregation and G_Y, with a thickness, $\delta_{INZ-I}(\theta)$, which is larger than the size of the SSN zone, δ_{SSN}. The other part is outside of the boundary plane of $r = r_{INZ-II}$, where the local temperature, $T(r)$ is equal to the critical nucleation temperature of the melt, T_n. T_n is slightly lower than the local liquidus temperature, $T_l(r)$. In the melt between these two INZ regions, nucleation of new grains is possible. This region is termed as the active nucleation zone (ANZ). In the direction towards the lower temperature side ($\theta = \pi$), due to the negative temperature gradient, the thickness of INZ is smaller than that of the SSN zone, $\delta_{INZ-I}(\theta) < \delta_{SSN}$. In this direction, the liquid metal has the smallest thickness of the INZ when the impingement between the solute segregation zone of the present grain, and that of the previously formed grains in the lower temperature region is ignored.

As shown in Fig. 11, for an arbitrary direction with an angle θ to G_Y ($0 \leq \theta \leq \pi$), the local melt temperature is given by:

$$T(r) = T_l^0 - \Delta T + (r - R_g) \cdot G_Y \cdot cos\theta, \quad (3)$$

where T_l^0 is liquidus temperature of the alloy.

With the local liquidus temperature of the melt around the grain obtained from Eq. (1), the local undercooling $\Delta T(r)$ can be calculated as:

$$\Delta T(r) = T_l(r) - T(r) = T_l(r) - T_l^0 + \Delta T - (r - R_g) \cdot G_Y \cdot cos\theta \cdot \quad (4)$$

The active nucleation zone is determined as the volume in between the two boundary planes $r = r_{INZ-I}(\theta)$ and $r = r_{INZ-II}(\theta)$, where $r_{INZ-I}(\theta)$ is the lower boundary plane, and $r_{INZ-II}(\theta)$ is the upper boundary plane of the ANZ. The values of $r_{INZ-I}(\theta)$ and $r_{INZ-II}(\theta)$ can be determined by $\Delta T(r) = \Delta T_{fg}$, where ΔT_{fg} is the minimum free growth undercooling needed for the available inoculant particles in the melt to initiate new free growth grains. Thus, the total volume fraction of the INZ is determined by:

$$f_{INZ} = \left\{ \sum_{i=1}^{N} \left[n_i \cdot \int_0^{\pi} \pi (r_{INZ-I}(\theta) \cdot sin\theta)^2 d(r_{INZ-I}(\theta) \cdot |cos\theta|) \right] + Vol_{INZ-II} \right\} \quad (5)$$
$$/Vol_{domain},$$

where $\int_0^{\pi} \pi (r_{INZ-I}(\theta) \cdot sin\theta)^2 d(r_{INZ-I}(\theta) \cdot |cos\theta|)$ is the volume of the inhibited nucleation zone around one grain that enclosed by r_{INZ-I} in 3-D space, the 2-D projection of which is shown in Fig. 11b as the red region marked with INZ-I. *i* is the class number of grains, *N* is the total size classes of nucleated grains, and n_i is the number of the solid grains of size class *i*. Vol_{INZ-II} and Vol_{domain} are the volume of the INZ-II (red region marked with INZ-II in Fig. 11b) and volume of the whole calculation domain, respectively. Eq. (5) can be solved by numerical integration in the model.

It should be noted that when $\theta = \pi/2$ or $G = 0$, Eq. (5) will become $f_{INZ} = \left(\sum_{i=1}^{N} \frac{4}{3} \pi (r_{SSN})_i^3 n_i \right) / V_{domain}$, which is identical to the fraction of the SSN in the isothermal melt solidification case. Therefore, Eq. (5) is a general equation for both isothermal melt solidification and directional solidification. In addition, f_{INZ} depends upon the diameter of the specific inoculant particle under consideration (namely, the size class of particles, *j*) since the free undercooling ΔT_{fg} required for successful initiation of a grain on a given TiB_2 particle is related to the particle diameter *d* by the free growth criterion [5].

Assuming the inoculant particles are uniformly distributed in the melt, only those lying in the active nucleation zone are able to initiate new grains, while the rest are inhibited. Therefore, the number of newly activated inoculation particles (thus the number of newly formed grains) from particle size class *j* at each time step, Δn_j is given by:

$$\Delta n_j = (1 - f_{INZ}) N(d)_j - n_{0_j}, \quad (6)$$

where $N(d)_j$ is the total number of inoculant particles in size class *j* of inoculant particles in the whole domain, and n_{0_j} is the number of particles in this class that have nucleated grains in the domain. In addition, these newly nucleated grains are assigned to a new size class of grains.

It should be noted that the solidification condition in Fig.11 is for $G \leq \Delta T/\delta_c$, where δ_c is the thickness of the solute diffusion layer. For the cases with $G > \Delta T/\delta_c$, the INZ-II region will move close to the growing grain and the volume of the ANZ will be

reduced. Therefore, the nucleation rate of grains in front of growing grains will be decreased. At high enough *G*, the fraction of the ANZ will become zero and the nucleation of new grains will be completely suppressed, thus the formed grains will grow into a columnar dendritic morphology.

4.2. Grain growth

After nucleation, it is assumed that the new grain grows in a spherical (globular) shape in the initial stage as described by Maxwell and Hellawell [11], and Greer et al. [5]. According to the stability criterion proposed by Mullins and Sekerka [63], the spherical growth would become unstable, and the grain morphology would transform into dendritic when the radius reaches a critical value. The equiaxed growth model including the globular to dendritic transition (GDT) is the same as the one developed in a previous work [12]. The detailed governing equations for keeping mass, volume and solute balance can be found in Ref. [12], here only some basic information is given.

For globular grains, only two region or phases are defined, namely a fully solid and a liquid phase. For each equiaxed dendritic grain cell, three regions or phases are discriminated, namely solid phase, interdendritic liquid phase inside the grain envelope, and extradendritic liquid phase outside the envelope. It is assumed that the concentration in the interdendritic liquid phase is uniform and equal to the liquid concentration at the dendritic tip, C_l^*.

The growth rate of globular grain $V_{g,i}$ in size class *i*, is given by [46, 64]:

$$V_{g,i} = \frac{dR}{dt} = \frac{D_l \cdot \Omega_i}{R_{g,i}}, \tag{7}$$

where $R_{g,i}$ is the radius of growing grains in size class *i*, D_l is the solute diffusion coefficient in liquid Al, and Ω_i is the solute supersaturation ratio of grain class *i*:

$$\Omega_i = \frac{C_{l,i}^* - C_l}{C_{l,i}^*(1-k)}, \tag{8}$$

where k is the partition coefficient of solute element, C_l the average solute concentration in the bulk melt and $C_{l,i}^*$ the liquid concentration at the solid-liquid interface of grain class i.

The dendrite tip growth velocity, $V_{d,i}$, is calculated by the model proposed by Kurz et al. [61], based on the hemispherical needle approximation to the dendrite tip:

$$V_{d,i} = \frac{D_l \cdot m \cdot (k-1) \cdot C_{l,i}^*}{2\pi^2 \cdot \Gamma} (\Omega_i)^2, \quad (9)$$

where m is the slope of liquidus line in phase diagram, and Γ is the Gibbs-Thomson coefficient.

4.3 Calculation of grain size

Heterogeneous nucleation and grain growth continue as solidification time increases and the calculation stops when nucleation ceases in the whole predefined calculation domain. Mathematically, $f_{INZ} = 1$ is the nucleation ceasing criterion. A maximum grain number, N_{tot}, in the whole calculation domain with the volume Vol_{domain} could be obtained and the final grain size $\overline{D}$ is approximated by [5]:

$$\overline{D} = \sqrt[3]{0.5/(N_{tot}/Vol_{domain})} \quad (10)$$

5. Modelling results

In this section, the proposed model is used to simulate the in-situ X-radiography solidification experiments of 0.05 wt.% Al-5Ti-1B inoculated Al-20Cu alloy under different temperature gradients and different constant cooling rates.

The physical parameters used in the numerical model are listed in Table 1. The size distribution of inoculant TiB_2 particles is based on the experimental measurement reported in a previous work [12]. The total number of potent TiB_2 particles per unit volume melt, for per addition of 0.1 wt.% Al-5Ti-1B, $N_0 = 2.5 \times 10^{11}\, m^{-3}$, tuned from a previous modeling study of an Al-10Cu alloy [12] is used in this study.

Fig. 12 shows the predicted and measured grain number density as a function of temperature gradient for the inoculated Al-20Cu alloy solidified at 0.1 and 0.5 K/s. As can be seen, at both cooling rates, the model reproduces the experimentally determined evolution trend of grain number density in relation to the temperature gradient and cooling rate. Taking into account that the added number of inoculant particles was taken from isothermal melt solidification simulations for Al-10Cu alloy [12], and no more tuning was done here, the agreement between the predicted and measured results is surprisingly good. In comparison to 0.1 K/s cooling rate, under 0.5 K/s cooling rate solidification conditions, the measured grain number density is less sensitive to the

temperature gradient. This has also been captured well by the present grain size prediction model. It proves that the proposed modeling approach to treat the inhibited nucleation zone and active nucleation zone around growing equiaxed grains under temperature gradient effects is indeed feasible.

The present model has also been tested in the high temperature gradient conditions. Fig. 13 shows the predicted propagation length of the nucleation front at nucleation stopping, and the corresponding grain number density of different solidification cases with temperature gradients ranging from 10-50 K/mm, and under a constant cooling rate of 0.025 K/s. It can be seen that the nucleation stops earlier while the grain number density decreases as G increases. For example, at G=40 K/mm, only a very limited number of grains could nucleate in the casting, but no more nucleation could happen ahead of the growth front at a growth length below 100 μm, indicating that columnar growth would dominate after nucleation ceasing. Therefore, the present model has the potential to predict the temperature gradient necessary for the transition from equiaxed to columnar grain growth. However, a quantitative validation is still necessary.

6. Discussion

The effect of temperature gradient G and growth velocity V on CET during unidirectional ingot casting or Bridgman type directional solidification of aluminum alloys has been investigated extensively either in-situ or post-situ. It is well accepted that during CET, the equiaxed grains nucleate in the constitutional undercooling zone in front of the steady-state growing columnar dendrites, where the constitutional undercooling provides the necessary nucleation undercooling of grains on inoculant particles. However, for normal casting of well-inoculated aluminum alloys, the bulk solidification process is dominated by nucleation and growth of equiaxed grains, and columnar dendritic grains are rarely observed, except for in the surface layer of shape castings, or chill surface of casting ingots (for example, DC-casting). Even in such regions, it is difficult for the columnar grains to reach a stead state grain growth. Instead, they are in the transient growth stage, which is close to the elongated dendritic grains shown in the in-situ experiments in this study.

However, only few studies have been focused on the effect of G on heterogeneous nucleation of grains and grain size of inoculated aluminum alloys. The in-situ X-radiographic results presented herein, clearly show that the existence of temperature

gradient enhances the preferential growth of grains along temperature gradient direction, reducing the heterogeneous nucleation rate and consequentially to an increase of the final grain size of castings. However, even at an extremely low cooling rate, 0.025 K/s, and a temperature gradient of 5 K/mm, most of the grains show nearly equiaxed morphology while no steady state columnar grain growth could be reached. This is due to the nucleation of new grains in front of the dendrite tips of growing grains, which stops further growth of the existing grains by soft impingement mechanism. Another important finding of the experimental study is that the temperature gradient effect on the grain morphology and grain size can be compensated by the cooling rate. The difference in grain number density between the near-isothermal melt solidification and directional solidification of the in-situ studies decreases with increasing cooling rate.

One of the biggest challenges to predict grain size of the well-inoculated directional castings is the rigorous treatment of the heterogeneous nucleation of grains under the effect of the temperature gradient. In the previous grain size prediction models on directional solidification, the nucleation of grains has been treated locally as an isothermal melt solidification condition [40, 42, 45, 46], by which the temperature gradient effect on nucleation was ignored. As illustrated by the schematic drawing in Fig. 11, the temperature gradient does have a strong effect on nucleation by increasing the fraction of INZ when the G value is high. The nucleation of grains both along the X and negative Y will be stopped by solute segregation stifling. The nucleation along the positive Y will be controlled by the volume of the ANZ. As G increases, the available undercooling in the local melt decreases and thus the volume of the ANZ reduces, which would hinder the nucleation of equiaxed grains. When G is large enough, the volume fraction of the ANZ will be reduced down to zero. Then the nucleation process in the directional casting is completely stopped, and a columnar dendrite growth will most likely happen. This is exactly the simulated cases shown in Fig. 13.

By using the equiaxed dendritic grain growth model based on hemispherical dendrite tip growth kinetics, the numerical model has well reproduced the influence of temperature gradient and cooling rate. Furthermore, the predicted grain number density is quantitatively in a good agreement with the experimental results. It verifies the feasibility of the method to calculate the volume fraction of the ANZ proposed in this work.

It is worth noting that in the model the nucleation of new grains on inoculant particles is purely controlled by the available undercooling in the local melt. When the total undercooling is equal or larger than the free growth undercooling needed for an inoculant particle, a new grain will form. In this case, the existence of a larger constitutional undercooling zone does not help the nucleation but will reduce the fraction of ANZ and thus hinder the further nucleation of grains. Based on the schematic drawing in Fig. 11, one can imagine that a thinner solute segregation layer, namely a smaller δ_c (for example caused by low diffusion rate of solute elements or by intensive melt shearing) will favor the nucleation of grains. This is also true for the isothermal melt solidification with constant cooling rate since the size of the ANZ is increased due to the decreasing of the solute segregation layer. Nevertheless, the segregation of solutes in the surrounding melt of growing grains will reduce the growth velocity of the dendrite tip and give more time, and accordingly more thermal undercooling for the nucleation of new grains on inoculant particles in front of the growing grains. In this sense, the constitutional undercooling and the growth restriction effects coming from the solutes will facilitate the nucleation of grains. Moreover, the available undercooling and size of the ANZ are also determined by the cooling rate. A high cooling rate or a fast heat extraction promote the formation of a larger bulk melt undercooling and a larger fraction of the ANZ.

It has to be noted that the present model is based on equiaxed grain growth and can not predict the columnar grain growth and the grain morphology change from equiaxed to elongated. A better treatment of grain growth with coupled solute diffusion calculation can be realized using modified Cellular Automaton model [28, 69, 70]. For grain size prediction of real castings, the convection of melt, varying cooling rate and temperature gradient, as well as the flotation of grains and inoculant particles have to be taken into account, which needs multiscale modeling approaches. The present work provides an approach to treat the influence of temperature gradient on grain nucleation for those comprehensive solidification models.

7. Conclusions

A quantitative study on the isolated temperature gradient effect and cooling rate effect on the heterogeneous nucleation and grain growth during directional solidification of inoculated Al alloys has been realized by using an in-situ X-ray radiographic solidification study.

The key findings are: the propagation velocity of the nucleation front in the directional casting is following the liquidus temperature line and approximately equal to $\dot{T}/G$; the existence of temperature gradient reduces the heterogeneous nucleation rate, promotes elongated grain growth and increases the final grain size; these effects increase with increasing temperature gradient when the cooling rate is kept constant. It is also found, however, that the temperature gradient effect on grain nucleation and grain growth can be reduced by increasing cooling rate.

A physical model is proposed to quantitatively address the temperature gradient effect on the heterogeneous nucleation of grains in the melt surrounding the growing grains, in terms of active nucleation zone (ANZ) and inhibited nucleation zone (INZ). Based on this model, a numerical model has been developed to predict the grain size for equiaxed directional solidification. The predicted grain size and number density of grains show a good agreement with the measurement results of in-situ solidification experiments. The model also has the capability to predict the temperature gradient necessary for the transition from equiaxed to columnar grain solidification. It confirms the importance of a rigorous treatment of the temperature gradient effect on the heterogeneous nucleation of grains in terms of INZ and ANZ for grain size prediction models. Such an approach can be applied for multiscale solidification structure simulation models.

Acknowledgements

This research work has been supported by a KPN Project, PRIMAL (project number: 236675/O30), in Norway. The financial support by The Research Council of Norway and industrial partners, Hydro Aluminium AS, Alcoa Norway AS is gratefully acknowledged.

References

[1] B.S. Murty, S.A. Kori, M. Chakraborty, Grain refinement of aluminium and its alloys by heterogeneous nucleation and alloying, Int. Mater. Rev. 47(1) (2002) 3-29.
[2] T.E. Quested, Understanding mechanisms of grain refinement of aluminium alloys by inoculation, Mater. Sci. Technol. 20(11) (2004) 1357-1369.
[3] M.A. Easton, M. Qian, A. Prasad, D.H. StJohn, Recent advances in grain refinement of light metals and alloys, Current Opinion in Solid State and Materials Science 20(1) (2016) 13-24.
[4] A.L. Greer, Overview: Application of heterogeneous nucleation in grain-refining of metals, J. Chem. Phys. 145(21) (2016) 211704.
[5] A.L. Greer, A.M. Bunn, A. Tronche, P.V. Evans, D.J. Bristow, Modelling of inoculation of metallic melts: application to grain refinement of aluminium by Al–Ti–B, Acta Mater. 48(11) (2000) 2823-2835.

[6] T.E. Quested, A.L. Greer, The effect of the size distribution of inoculant particles on as-cast grain size in aluminium alloys, Acta Mater. 52(13) (2004) 3859-3868.
[7] T.E. Quested, A.L. Greer, Athermal heterogeneous nucleation of solidification, Acta Mater. 53(9) (2005) 2683-2692.
[8] A.L. Greer, T.E. Quested, Heterogeneous grain initiation in solidification, Philos. Mag. 86(24) (2006) 3665-3680.
[9] J.A. Dantzig, M. Rappaz, Solidification, EFPL Press2009.
[10] T.E. Quested, A.T. Dinsdale, A.L. Greer, Thermodynamic modelling of growth-restriction effects in aluminium alloys, Acta Mater. 53(5) (2005) 1323-1334.
[11] I. Maxwell, A. Hellawell, A simple model for grain refinement during solidification, Acta Metall. 23(2) (1975) 229-237.
[12] Y. Xu, D. Casari, Q. Du, R.H. Mathiesen, L. Arnberg, Y. Li, Heterogeneous nucleation and grain growth of inoculated aluminium alloys: An integrated study by in-situ X-radiography and numerical modelling, Acta Mater. 140(Supplement C) (2017) 224-239.
[13] M. Johnsson, L. Backerud, G. Sigworth, Study of the mechanism of grain refinement of aluminum after additions of Ti- and B-containing master alloys, Metall. Trans. A 24(2) (1993) 481-491.
[14] M. Johnsson, Grain refinement of aluminium studied by use of a thermal analytical technique, Thermoch. Acta 256(1) (1995) 107-121.
[15] J.E.C. Hutt, A.K. Dahle, Y.C. Lee, D.H. StJohn, The effects of growth restriction and effective nucleant potency on grain size and morphology in Al-Si and Al-Cu alloys, in: C.E. Eckert (Ed.), Light Metals1999, Minerals, Metals & Materials Soc, Warrendale, 1999, pp.685-692.
[16] Y.C. Lee, A.K. Dahle, D.H. StJohn, J.E.C. Hutt, The effect of grain refinement and silicon content on grain formation in hypoeutectic Al–Si alloys, Mater. Sci. Eng. A 259(1) (1999) 43-52.
[17] A. Tronche, M. Vandyoussefi, A.L. Greer, Instability of TiC particles in aluminium melts inoculated with an Al-Ti-C grain refiner, Mater. Sci. Technol. 18(10) (2002) 1072-1078.
[18] T.E.Quested, Solidification of Inoculated Aluminium Alloys, University of Cambridge, Cambridge UK, 2004.
[19] R. Elliott, The Formation of the Equiaxed Crystal Zone During Ingot Solidification, The British Foundryman 57 (1964) 398-401.
[20] S. Kim, R.N. Grugel, The transition from columnar to equiaxed dendritic growth in proeutectic, low-volume fraction copper, Pb−Cu alloys, Metall. Trans. A 23(6) (1992) 1807-1815.
[21] T. Pollock, W. Murphy, The breakdown of single-crystal solidification in high refractory nickel-base alloys, Metall. Mater. Trans. A 27(4) (1996) 1081-1094.
[22] C.A. Siqueira, N. Cheung, A. Garcia, Solidification thermal parameters affecting the columnar-to-equiaxed transition, Metall and Mat Trans A 33(7) (2002) 2107-2118.
[23] H. Jung, N. Mangelinck-Noël, H. Nguyen-Thi, B. Billia, Columnar to equiaxed transition during directional solidification in refined Al-based alloys, J. Alloys Compd. 484(1–2) (2009) 739-746.
[24] D.A. Pineda, M.A. Martorano, Columnar to equiaxed transition in directional solidification of inoculated melts, Acta Mater. 61(5) (2013) 1785-1797.
[25] M. Gäumann, R. Trivedi, W. Kurz, Nucleation ahead of the advancing interface in directional solidification, Mater. Sci. Eng. A 226–228(0) (1997) 763-769.
[26] C.A. Gandin, From constrained to unconstrained growth during directional solidification, Acta Mater. 48(10) (2000) 2483-2501.
[27] M.A. Martorano, C. Beckermann, C.A. Gandin, A solutal interaction mechanism for the columnar-to-equiaxed transition in alloy solidification, Metall. Mater. Trans. A 34(8) (2003) 1657-1674.
[28] H.B. Dong, P.D. Lee, Simulation of the columnar-to-equiaxed transition in directionally solidified Al–Cu alloys, Acta Mater. 53(3) (2005) 659-668.
[29] A. Badillo, C. Beckermann, Phase-field simulation of the columnar-to-equiaxed transition in alloy solidification, Acta Mater. 54(8) (2006) 2015-2026.

[30] M.A. Martorano, V.B. Biscuola, Predicting the columnar-to-equiaxed transition for a distribution of nucleation undercoolings, Acta Mater. 57(2) (2009) 607-615.
[31] J.D. Hunt, Steady state columnar and equiaxed growth of dendrites and eutectic, Mater. Sci. Eng. 65(1) (1984) 75-83.
[32] M. Vandyoussefi, A.L. Greer, Application of cellular automaton–finite element model to the grain refinement of directionally solidified Al–4.15 wt% Mg alloys, Acta Mater. 50(7) (2002) 1693-1705.
[33] G. Reinhart, N. Mangelinck-Noël, H. Nguyen-Thi, T. Schenk, J. Gastaldi, B. Billia, P. Pino, J. Härtwig, J. Baruchel, Investigation of columnar–equiaxed transition and equiaxed growth of aluminium based alloys by X-ray radiography, Mater. Sci. Eng. A 413–414 (2005) 384-388.
[34] H. Nguyen-Thi, G. Reinhart, N. Mangelinck-Noël, H. Jung, B. Billia, T. Schenk, J. Gastaldi, J. Härtwig, J. Baruchel, In-Situ and Real-Time Investigation of Columnar-to-Equiaxed Transition in Metallic Alloy, Metall. Mater. Trans. A 38(7) (2007) 1458-1464.
[35] A. Prasad, L. Yuan, P.D. Lee, M. Easton, D. StJohn, The effect of the melt thermal gradient on the size of the constitutionally supercooled zone, IOP Conference Series: Materials Science and Engineering 117(1) (2016) 012001.
[36] P. Thévoz, J.L. Desbiolles, M. Rappaz, Modeling of equiaxed microstructure formation in casting, Metall. Trans. A 20(2) (1989) 311-322.
[37] P. Desnain, Y. Fautrelle, J.L. Meyer, J.P. Riquet, F. Durand, Prediction of equiaxed grain density in multicomponent alloys, stirred electromagnetically, Acta Metall. 38(8) (1990) 1513-1523.
[38] M.A. Easton, D.H. StJohn, A model of grain refinement incorporating alloy constitution and potency of heterogeneous nucleant particles, Acta Mater. 49(10) (2001) 1867-1878.
[39] A.L. Greer, T.E. Quested, J.E. Spalding, Modelling of grain refinement in directional solidification, in: W.A. Schneider (Ed.), Light Metals 2002, Minerals, Metals & Materials Soc, Warrendale, 2002, pp. 687-694.
[40] T.E. Quested, A.L. Greer, Grain refinement of Al alloys: Mechanisms determining as-cast grain size in directional solidification, Acta Mater. 53(17) (2005) 4643-4653.
[41] B. Böttger, J. Eiken, M. Apel, Phase-field simulation of microstructure formation in technical castings – A self-consistent homoenthalpic approach to the micro–macro problem, J. Comput. Phys. 228(18) (2009) 6784-6795.
[42] M. Qian, P. Cao, M.A. Easton, S.D. McDonald, D.H. StJohn, An analytical model for constitutional supercooling-driven grain formation and grain size prediction, Acta Mater. 58(9) (2010) 3262-3270.
[43] H. Men, Z. Fan, Effects of solute content on grain refinement in an isothermal melt, Acta Mater. 59(7) (2011) 2704-2712.
[44] D. Shu, B. Sun, J. Mi, P.S. Grant, A quantitative study of solute diffusion field effects on heterogeneous nucleation and the grain size of alloys, Acta Mater. 59(5) (2011) 2135-2144.
[45] D.H. StJohn, M. Qian, M.A. Easton, P. Cao, The Interdependence Theory: The relationship between grain formation and nucleant selection, Acta Mater. 59(12) (2011) 4907-4921.
[46] Q. Du, Y.J. Li, An extension of the Kampmann-Wagner numerical model towards as-cast grain size prediction of multicomponent aluminum alloys, Acta Mater. 71 (2014) 380-389.
[47] M. Martorano, D. Aguiar, J. Arango, Multigrain and Multiphase Mathematical Model for Equiaxed Solidification, Metall. Mater. Trans. A 46(1) (2015) 377-395.
[48] T.E. Quested, A.L. Greer, Modelling of microstructural evolution in Bridgman specimens, in: M.G. Chu, D.A. Granger, Q.Y. Han (Eds.), Solidification of Aluminum Alloys, TMS, 2004, pp. 43-55.
[49] D.R. Liu, N. Mangelinck-Noël, C.A. Gandin, G. Zimmermann, L. Sturz, H. Nguyen-Thi, B. Billia, Simulation of directional solidification of refined Al–7wt.%Si alloys – Comparison with benchmark microgravity experiments, Acta Mater. 93(Supplement C) (2015) 24-37.
[50] M. Rappaz, C.A. Gandin, Probabilistic modelling of microstructure formation in solidification processes, Acta Metall. Mater. 41(2) (1993) 345-360.

[51] C.A. Gandin, M. Rappaz, A coupled finite element-cellular automaton model for the prediction of dendritic grain structures in solidification processes, Acta Metall. Mater. 42(7) (1994) 2233-2246.
[52] W.U. Mirihanage, D.J. Browne, Combined analytical/numerical modelling of nucleation and growth during equiaxed solidification under the influence of thermal convection, Comput. Mater. Sci. 46(4) (2009) 777-784.
[53] M. Bedel, K.O. Tveito, M. Založnik, H. Combeau, M. M'Hamdi, A model study of the impact of the transport of inoculant particles on microstructure formation during solidification, Comput. Mater. Sci. 102(0) (2015) 95-109.
[54] A.G. Murphy, D.J. Browne, W.U. Mirihanage, R.H. Mathiesen, Combined in situ X-ray radiographic observations and post-solidification metallographic characterisation of eutectic transformations in Al–Cu alloy systems, Acta Mater. 61(12) (2013) 4559-4571.
[55] H. Nguyen-Thi, G. Reinhart, G. Salloum Abou Jaoude, R.H. Mathiesen, G. Zimmermann, Y. Houltz, D. Voss, A. Verga, D.J. Browne, A.G. Murphy, XRMON-GF: a novel facility for solidification of metallic alloys with in situ and time-resolved X-ray radiographic characterization in microgravity conditions, J. Cryst. Growth 374 (0) (2013) 23-30.
[56] C. Rakete, C. Baumbach, A. Goldschmidt, D. Samberg, C.G. Schroer, F. Breede, C. Stenzel, G. Zimmermann, C. Pickmann, Y. Houltz, C. Lockowandt, O. Svenonius, P. Wiklund, R.H. Mathiesen, Compact x-ray microradiograph for in situ imaging of solidification processes: Bringing in situ x-ray micro-imaging from the synchrotron to the laboratory, Rev. Sci. Instrum. 82(10) (2011) 105108.
[57] A.G. Murphy, W.U. Mirihanage, D.J. Browne, R.H. Mathiesen, Equiaxed dendritic solidification and grain refiner potency characterised through in situ X-radiography, Acta Mater. 95(0) (2015) 83-89.
[58] https://imagej.nih.gov/ij/index.html. (https://imagej.nih.gov/ij/index.html).
[59] A. Bogno, H. Nguyen-Thi, G. Reinhart, B. Billia, J. Baruchel, Growth and interaction of dendritic equiaxed grains: In situ characterization by synchrotron X-ray radiography, Acta Mater. 61(4) (2013) 1303-1315.
[60] D.G. Eskin, Physical metallurgy of direct chill casting of aluminum alloys, CRC press2008.
[61] W. Kurz, D.J. Fisher, Fundamentals of Solidification, 4th ed., Trans Tech Publication LTD1998.
[62] H.B. Aaron, D. Fainstein, G.R. Kotler, Diffusion-Limited Phase Transformations: A Comparison and Critical Evaluation of the Mathematical Approximations, J. Appl. Phys. 41(11) (1970) 4404-4410.
[63] W.W. Mullins, R.F. Sekerka, Morphological Stability of a Particle Growing by Diffusion or Heat Flow, J. Appl. Phys. 34(2) (1963) 323-329.
[64] M. Wu, A. Ludwig, Modeling equiaxed solidification with melt convection and grain sedimentation—I: Model description, Acta Mater. 57(19) (2009) 5621-5631.
[65] Ø. Nielsen, A. Mo, B. Appolaire, H. Combeau, Measurements and modeling of the microstructural morphology during equiaxed solidification of Al-Cu alloys, Metall. Mater. Trans. A 32(8) (2001) 2049-2060.
[66] M. Wu, A. Ludwig, Modeling equiaxed solidification with melt convection and grain sedimentation—II. Model verification, Acta Mater. 57(19) (2009) 5632-5644.
[67] Y. Du, Y.A. Chang, B. Huang, W. Gong, Z. Jin, H. Xu, Z. Yuan, Y. Liu, Y. He, F.Y. Xie, Diffusion coefficients of some solutes in fcc and liquid Al: critical evaluation and correlation, Mater. Sci. Eng. A 363(1–2) (2003) 140-151.
[68] Q. Du, Y.J. Li, Prediction of As-Cast Grain Size of Inoculated Multicomponent Aluminum Alloys, Mater. Sci. Forum 790-791 (2014) 185-190.
[69] X. Zhang, J. Zhao, H. Jiang, M. Zhu, A three-dimensional cellular automaton model for dendritic growth in multi-component alloys, Acta Mater. 60(5) (2012) 2249-2257.
[70] M.F. Zhu, C.P. Hong, A Modified Cellular Automaton Model for the Simulation of Dendritic Growth in Solidification of Alloys, ISIJ Int. 41(5) (2001) 436-445.

In-situ X-radiography

G=10 K/mm

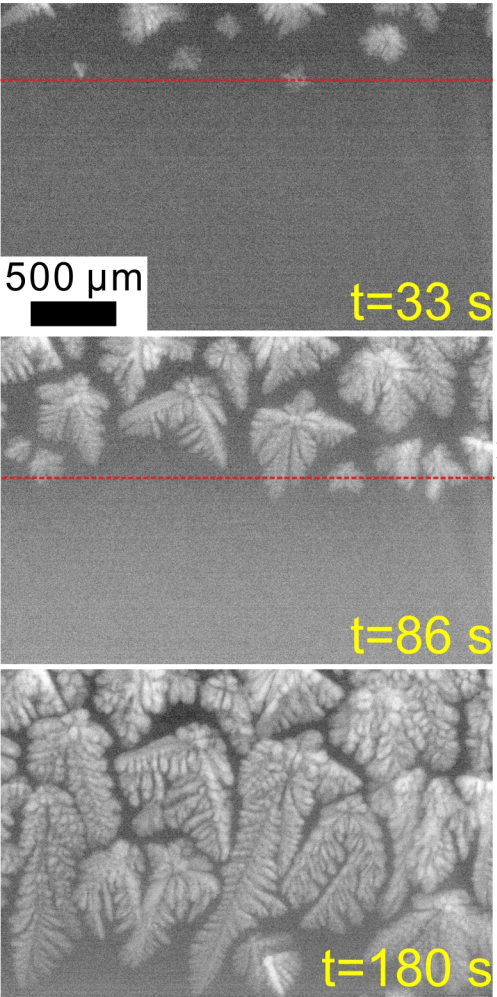

Modeling

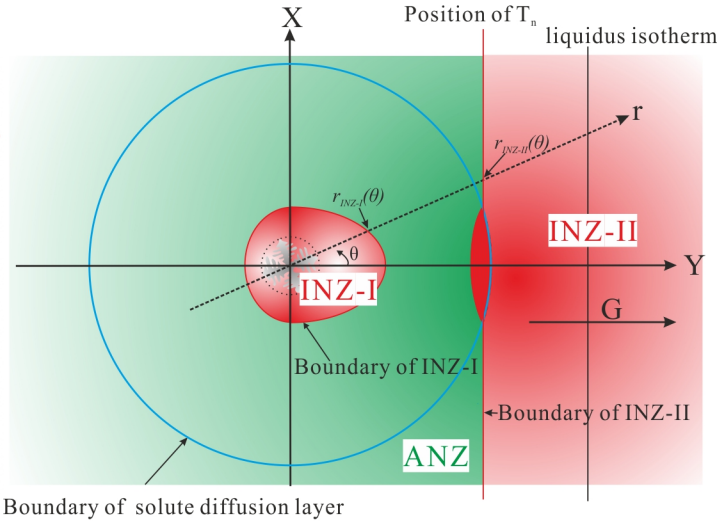

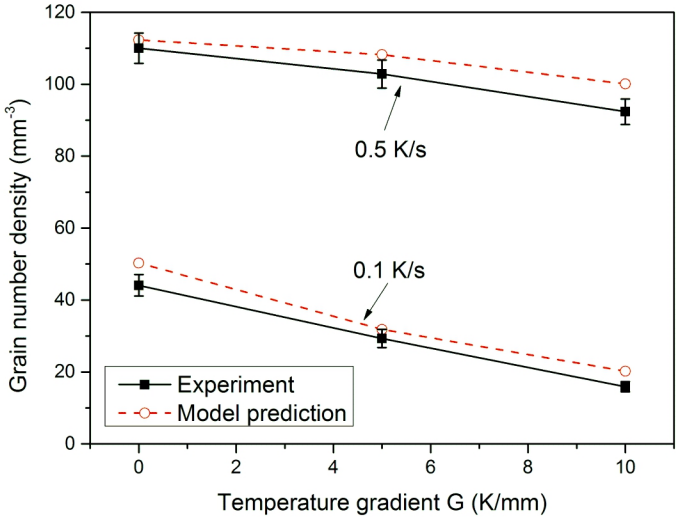

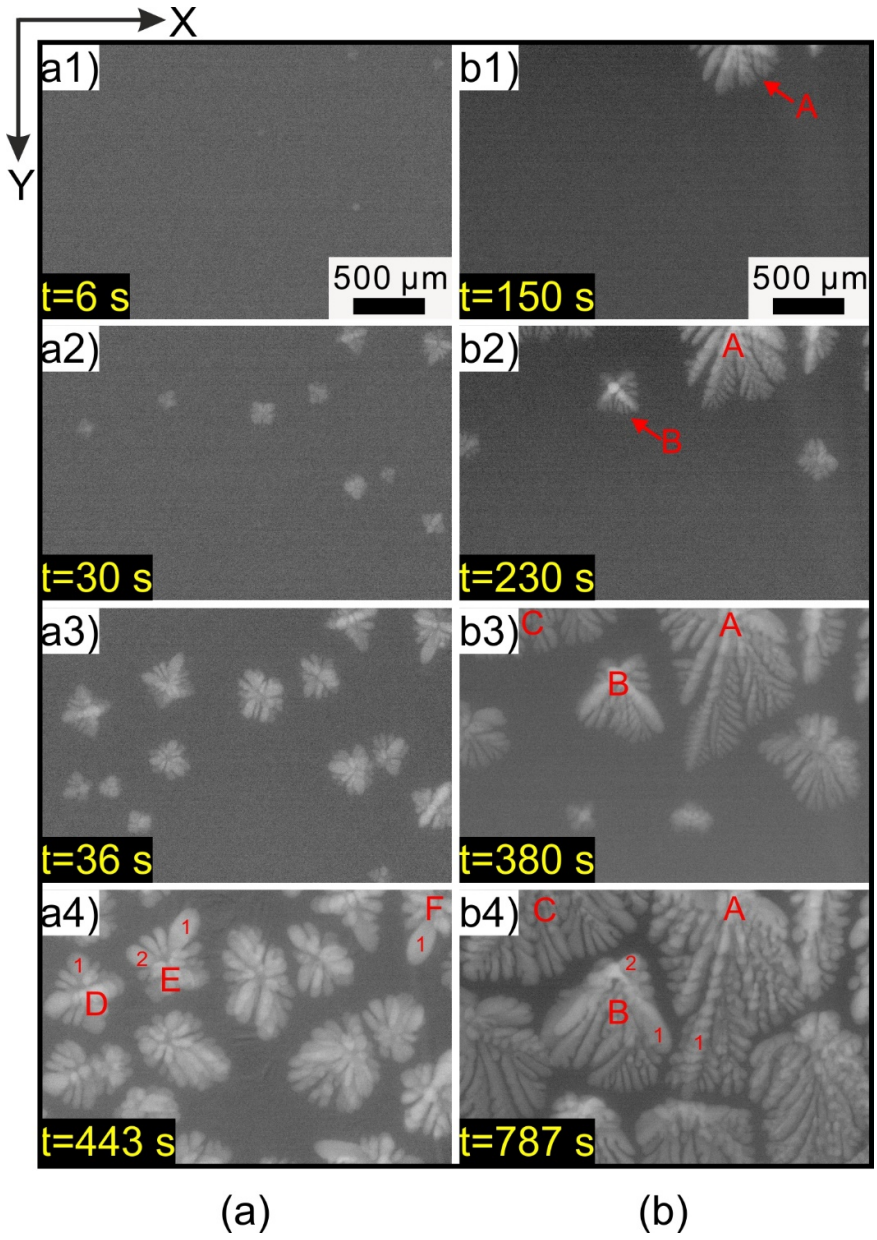

Fig. 1. Selected X-radiographic images from in-situ studies of solidification of inoculated Al-20Cu alloy under the same cooling rate of 0.025 K/s but with two different temperature gradients G: (a) near-isothermal solidification with $G_Y \cong 0$ and (b) directional solidification with $G_Y = 5$ K/mm.

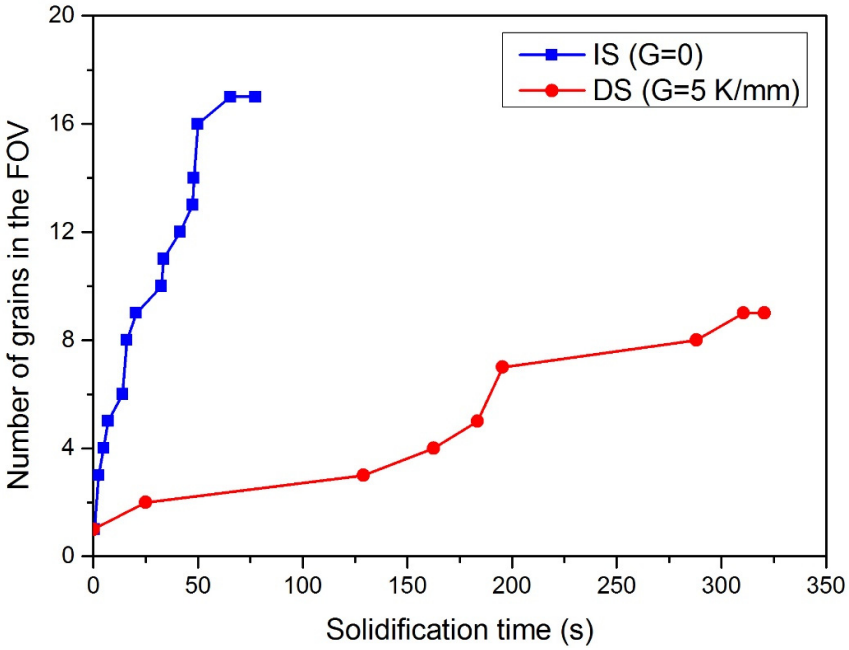

Fig. 2. Evolution of the total number of grains in the FOV as a function of solidification time since the first grain appears in the FOV in two solidification cases, near-isothermal solidification ($G_Y \cong 0$) and directional solidification (G_Y=5 K/mm) shown in Fig. 1 ($\dot{T}$=0.025 K/s).

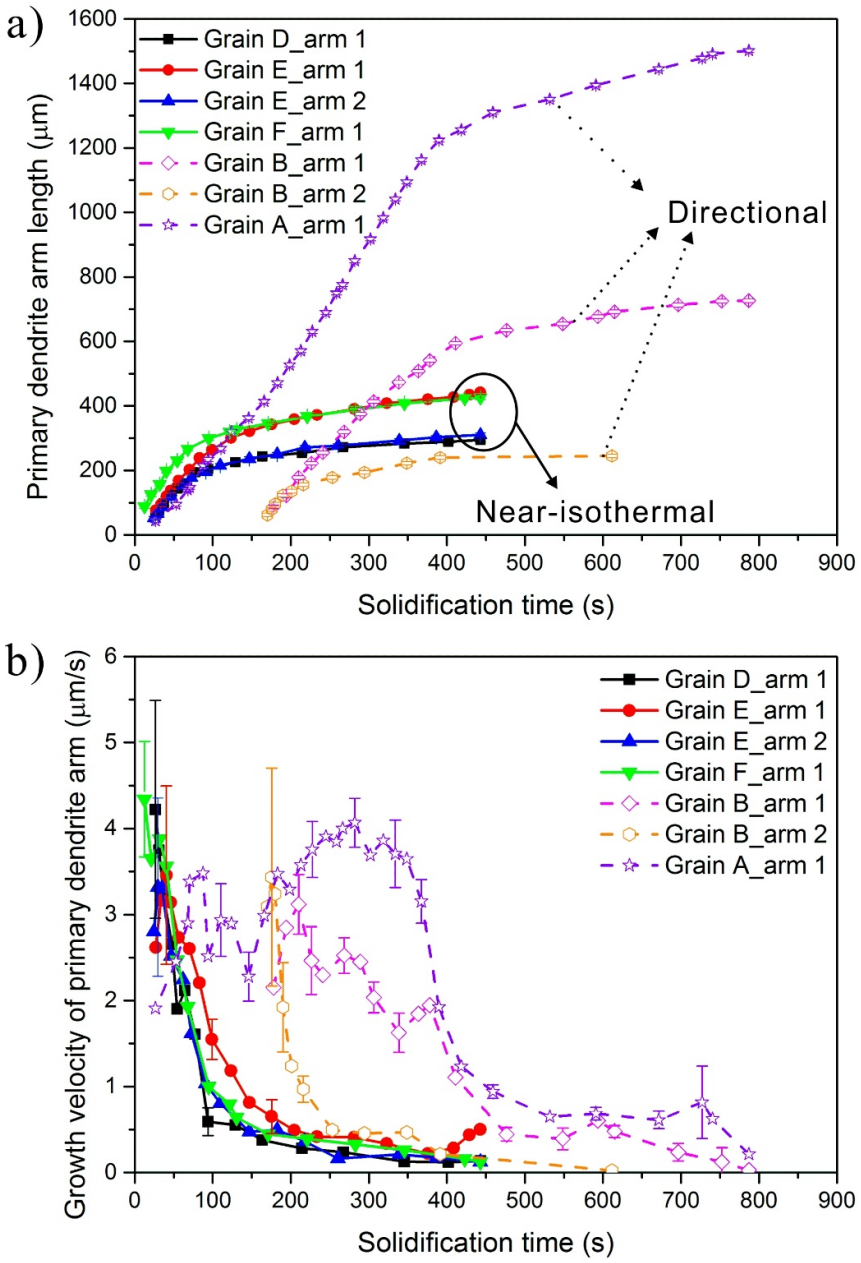

Fig. 3. (a) Evolution of individual primary dendrite arm length over time (Error bars denote 4 pixels, ±5.7 μm) and (b) corresponding growth velocity for several grains selected from in-situ X-radiographic images (labeled in Fig. 1, $\dot{T}$=0.025 K/s) in two solidification conditions: near-isothermal solidification ($G_Y \cong 0$) and directional solidification (G_Y=5 K/mm). Error bars are only drawn for some data points for clarity.

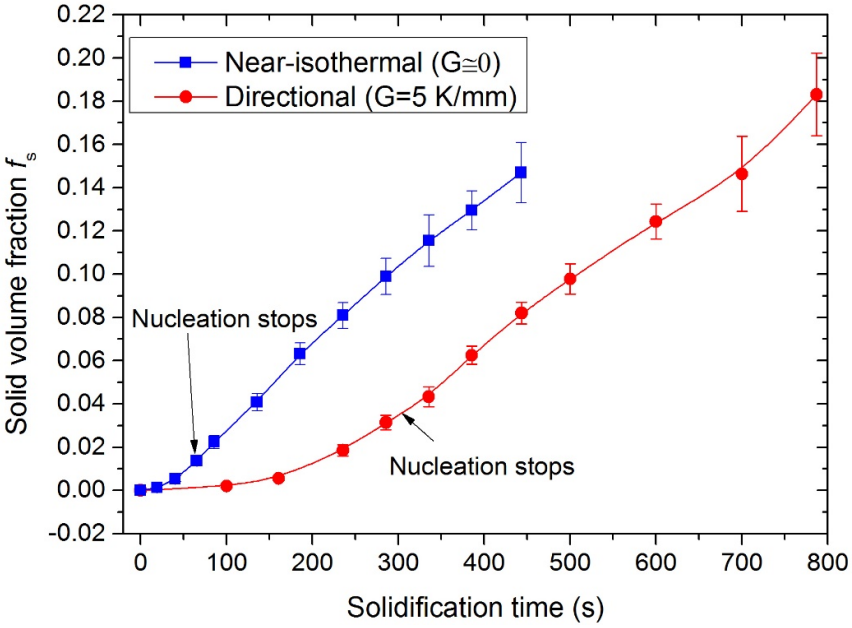

Fig. 4. Evolution of the solid volume fraction as a function of solidification time since the first grain appears in the FOV in two solidification cases, near-isothermal solidification ($G_Y \cong 0$) and directional solidification (G_Y=5 K/mm) shown in Fig. 1 ($\dot{T}$=0.025 K/s).

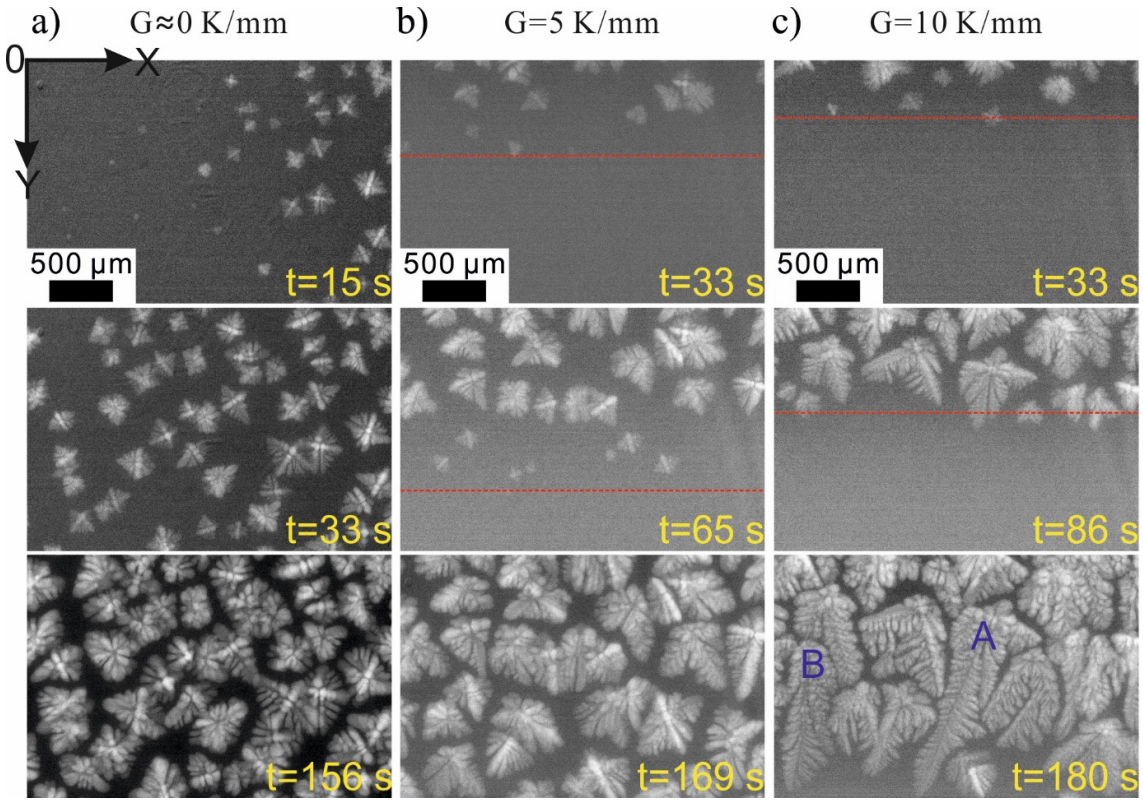

Fig. 5. Selected X-radiographic images from in-situ studies of solidification of inoculated Al-20Cu alloy at 0.1 K/s cooling rate under three different temperature gradients G: (a) $G_Y \cong 0$, (b) G_Y=5 K/mm and (c) G_Y=10 K/mm. The dashed red lines in (b) and (c) indicate the position of the nucleation front.

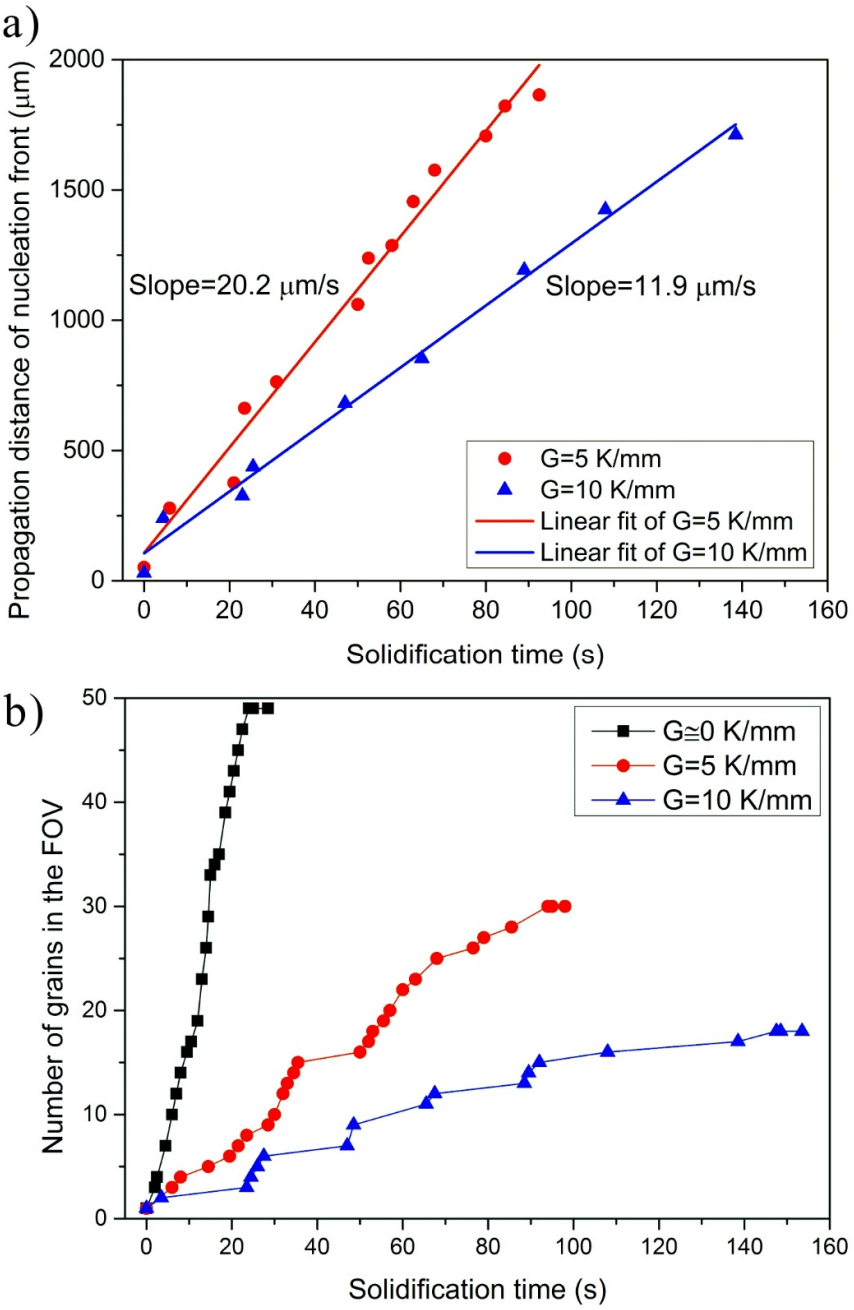

Fig. 6. (a) Propagation distance of the nucleation front (indicated by the red dashed lines in Fig. 5) in the Y-direction as a function of solidification time for directional solidification shown in Fig. 5 (Error bars ±5.7 μm not shown for clarity). (b) Evolution of the total number of grains in the FOV as a function of solidification time in three solidification cases shown in Fig. 5 ($\dot{T}$ =0.1 K/s, G=0, 5, 10 K/mm).

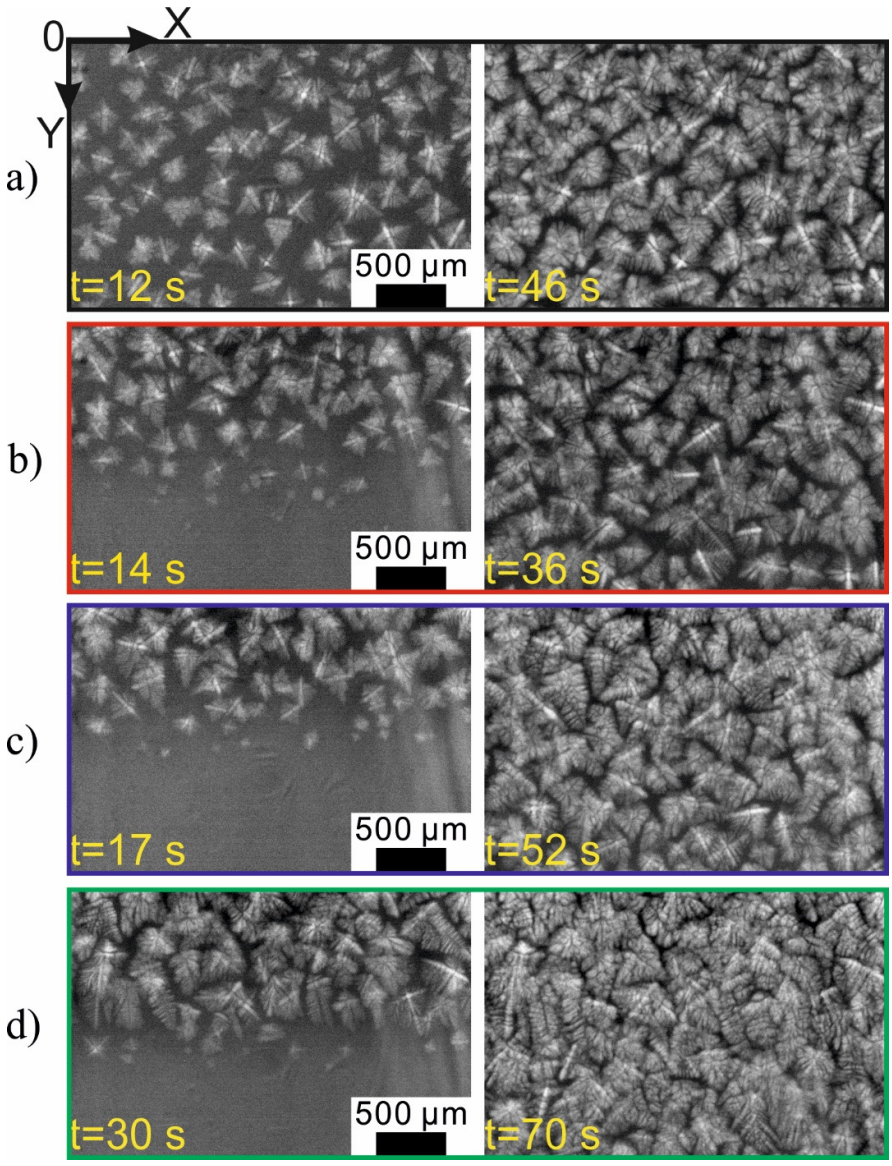

Fig. 7. Selected X-radiographic images during solidification of inoculated Al-20Cu alloy at a constant cooling rate of 0.5 K/s, with different temperature gradients G, (a) G_Y=0, (b) G_Y=5 K/mm, (c) G_Y=10 K/mm, and (d) G_Y=15 K/mm.

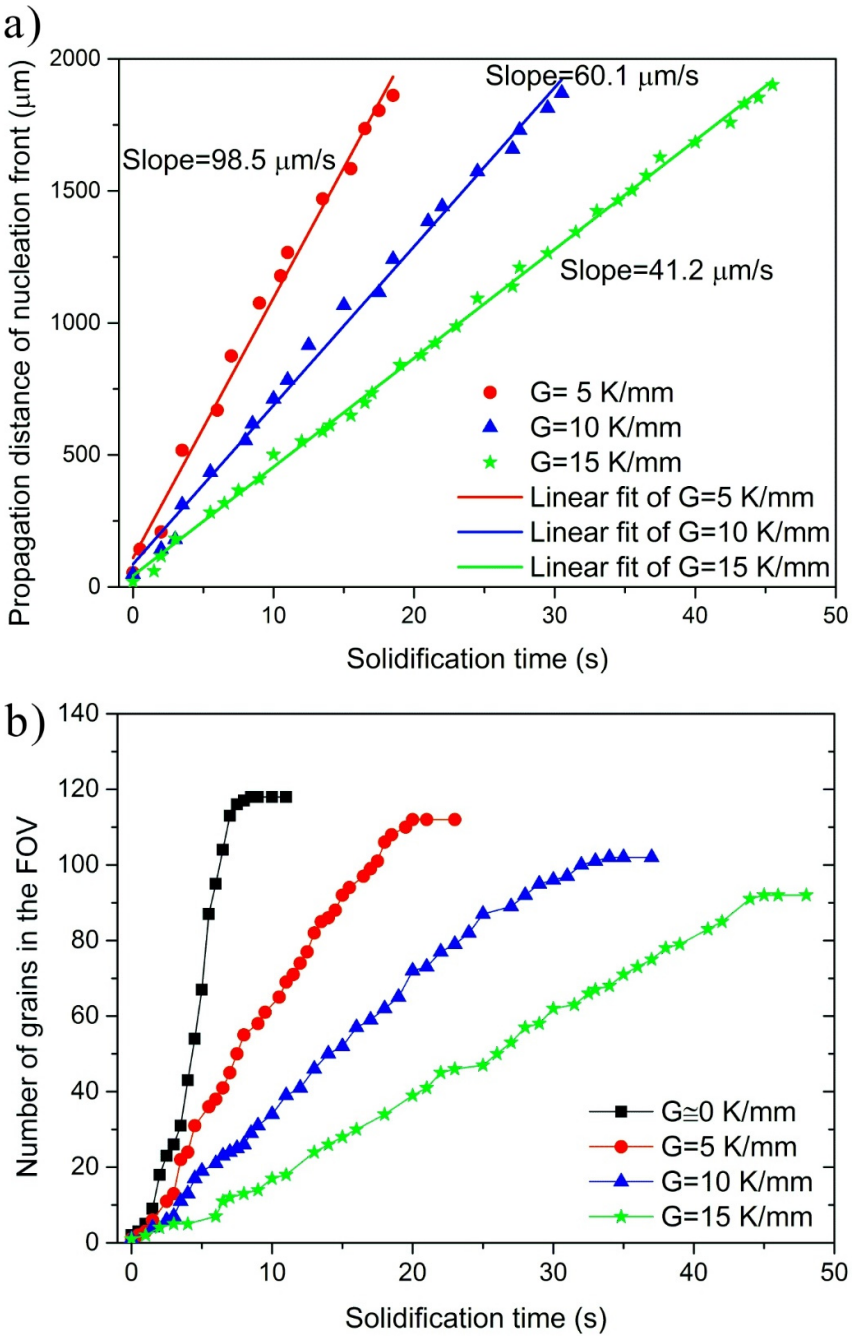

Fig. 8. (a) Propagation distance of the nucleation front in the Y-direction as a function of solidification time for the in-situ directional solidification experiments shown in Fig. 7 (Error bars ±5.7 μm not shown for clarity). (b) Evolution of the number of grains in the FOV with solidification time for solidification cases shown in Fig. 7 ($\dot{T}$ =0.5 K/s, G=0, 5, 10, 15 K/mm).

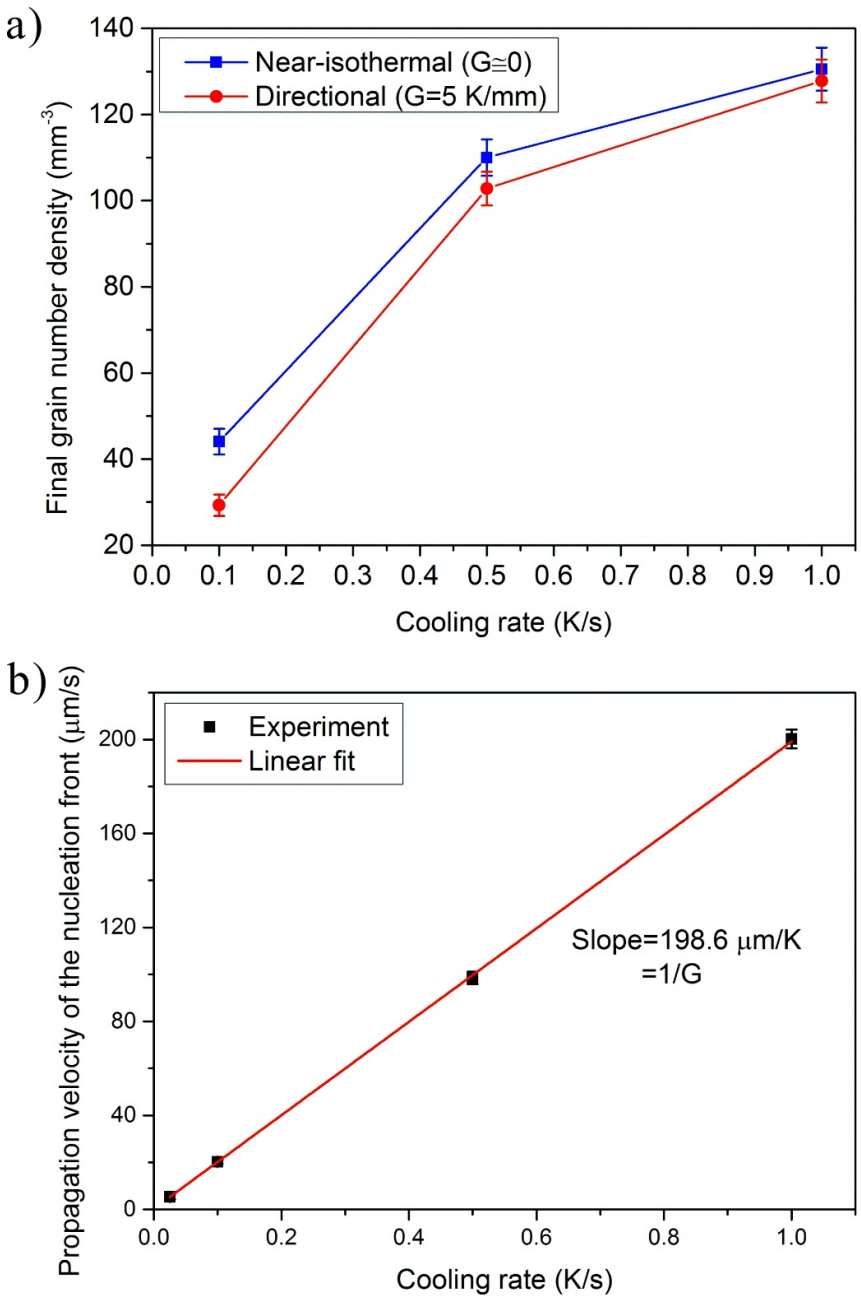

Fig. 9. (a) Final grain number density of the inoculated Al-20Cu alloy sample as a function of cooling rate in two different solidification cases: near-isothermal solidification and directional solidification with G=5 K/mm. (b) Propagation velocity of the nucleation front as a function of cooling rate in directional solidification with G=5 K/mm.

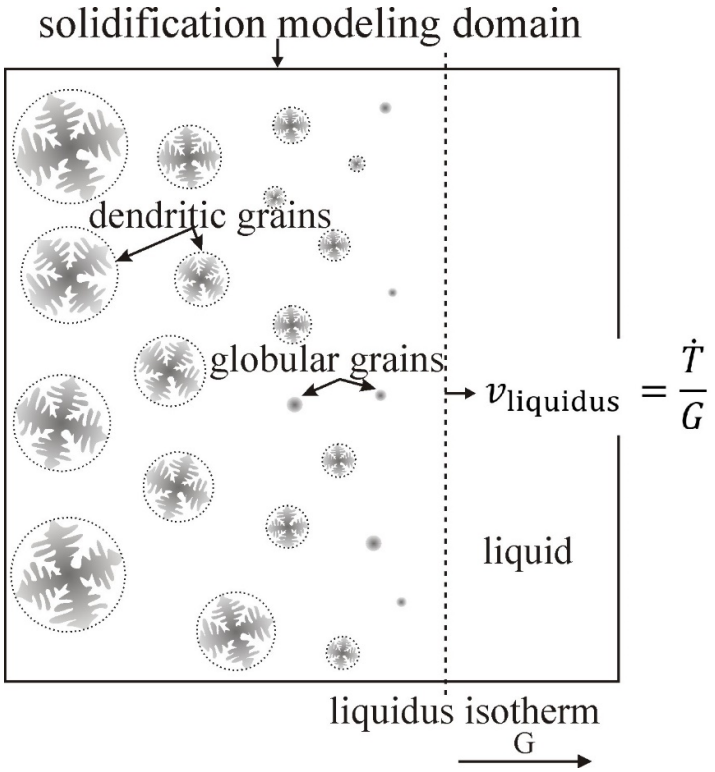

Fig. 10. Schematic illustration of the solidification modeling domain (2-D section along G) and the heterogeneous nucleation and grain growth behavior in the domain. Both globular and dendritic grains are simulated, and the dashed line represents the liquidus isotherm.

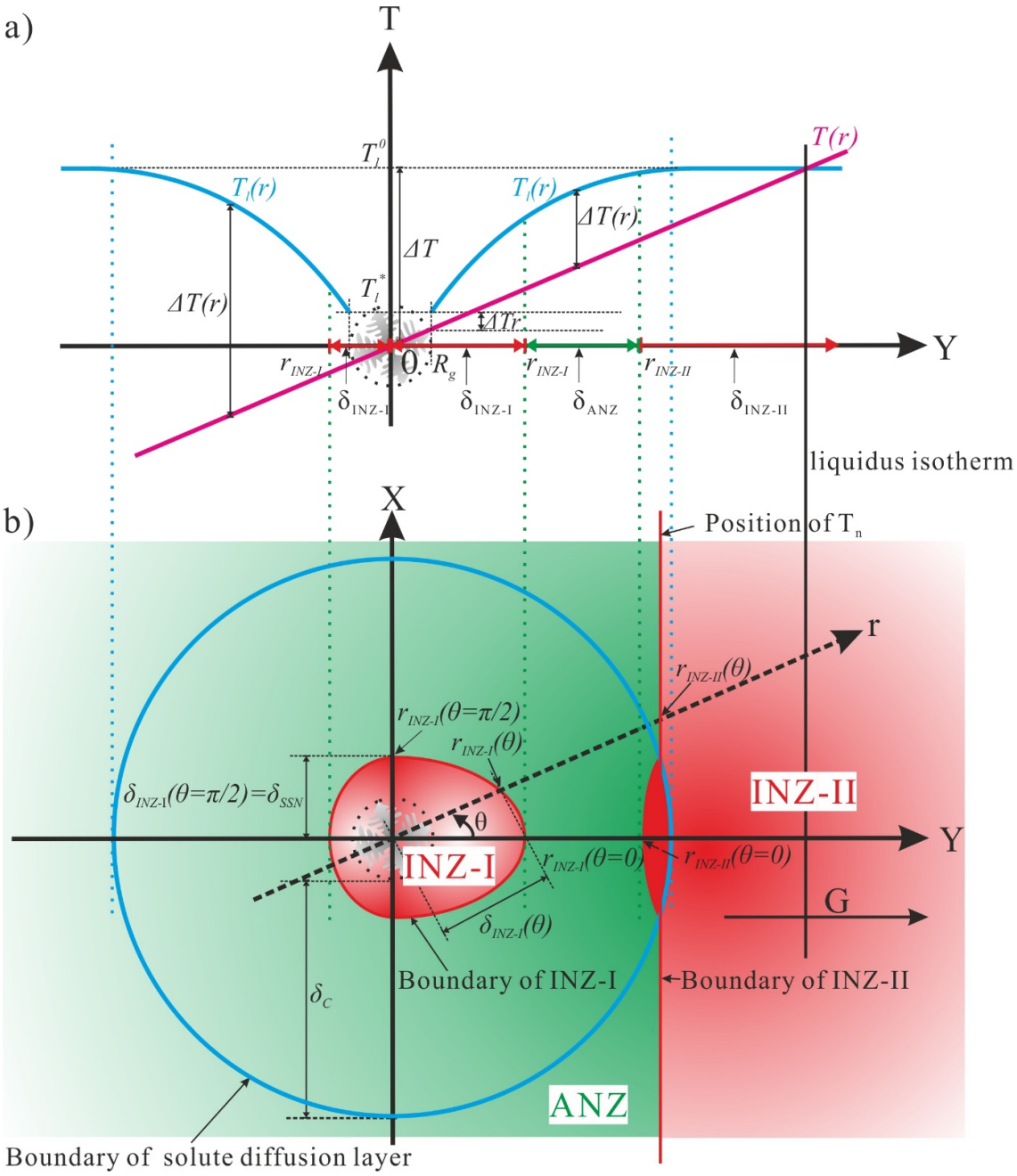

Fig. 11. Schematic drawing to show the influence of temperature gradient on the nucleation of new grains around one single grain. (a) Liquidus temperature $T_l(r)$, melt temperature $T(r)$ and the corresponding local undercooling of the liquid $\Delta T(r)$ outside the grain envelope that along the temperature gradient direction. (b) 2-Dimensional illustration of the inhibited nucleation zone (INZ), active nucleation zone (ANZ), and the corresponding boundary.

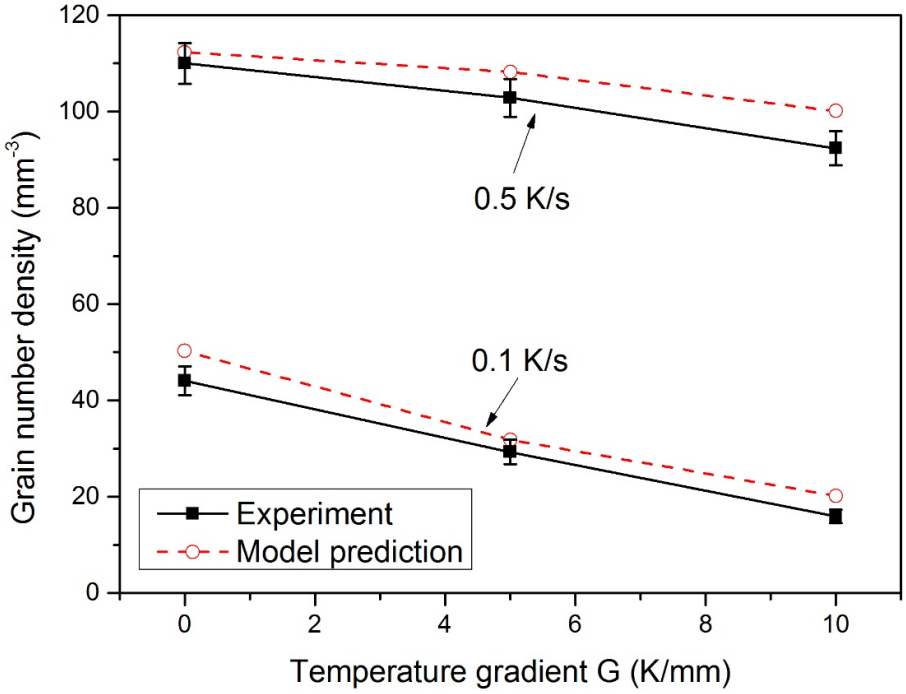

Fig. 12. Predicted and measured grain number density of the inoculated Al-20Cu alloy as a function of temperature gradient in the solidification cases of 0.1 K/s and 0.5 K/s cooling rate.

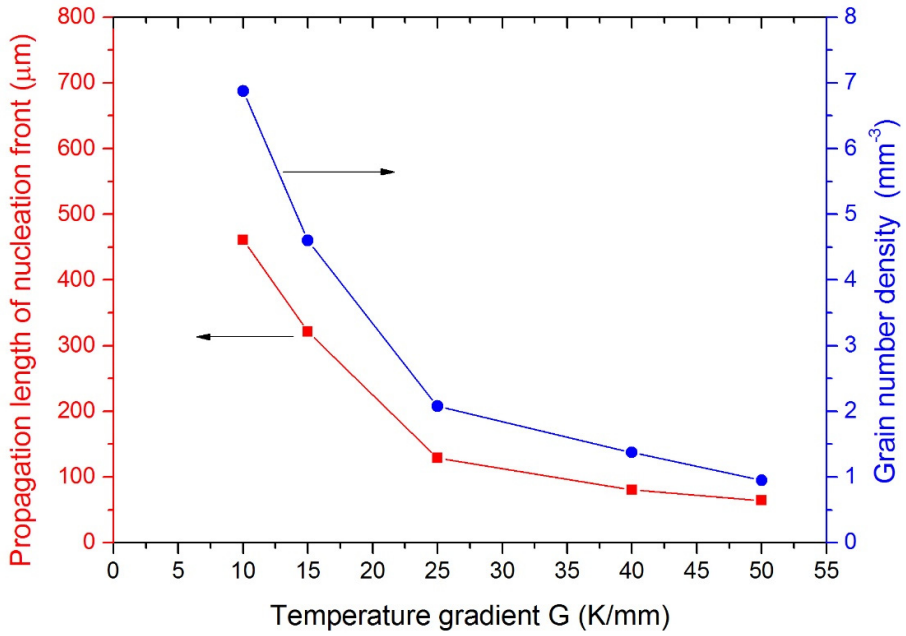

Fig. 13. Predicted propagation length of nucleation front at nucleation stopping and grain number density in the modeling domain as a function of temperature gradient in the directional solidification of the inoculated Al-20Cu alloy under 0.025 K/s cooling rate.

Table 1 Physical parameters used in the model for the Al-20Cu alloy.

Quantity	Symbol	Units	Value	Ref.
Gibbs-Thomson coefficient	Γ	m K	2.41×10^{-7}	[47, 65, 66]
Diffusivity in Al melt (Cu)	D_l	$m^2\ s^{-1}$	4.65×10^{-9}	[67, 68]
Liquidus slope	m	K wt.%$^{-1}$	-3.4	[68]
Partition coefficient	k		0.14	[68]

Appendix

Nomenclature

C_0	bulk melt composition (wt.%)
C_l	average solute concentration in the bulk melt
C_l^*	solute concentration in the liquid at the solid/liquid interface (wt.%)
$C_{l,i}^*$	liquid concentration at the solid-liquid interface of grain class i (wt.%)
d	particle diameter
D_l	solute diffusion coefficient in liquid Al ($m^2\ s^{-1}$)
$\overline{D}$	average grain size (m or μm)
f_{INZ}	total volume fraction of inhibited nucleation zone
G	temperature gradient (K/mm or K/m)
G_Y	temperature gradient along the Y-direction (K/mm or K/m)
i	Specific size class of the grains
j	Specific size class of the particles
k	partition coefficient of solute element
m	slope of liquidus line in phase diagram ($K\ wt.\%^{-1}$)
n_i	number of the solid grains of size class *i*
N	total size classes of nucleated grains
Δn_j	number of newly activated inoculation particles (thus the number of newly formed grains) from particle size class *j* at each time step
$N(d)_j$	total number of inoculant particles in size class *j* of inoculant particles in the whole domain
$n_{0\,j}$	number of particles in this class *j* that have nucleated grains in the domain
N_{tot}	maximum grain number in the whole calculation domain
r	distance to the center of the grain (m or μm)
$r_{INZ-I}(\theta)$	boundary position of INZ-I or distance of INZ-I to the center of the grain in θ direction (m or μm)
$r_{INZ-II}(\theta)$	boundary position of INZ-II or distance of INZ-II to the center of the grain in θ direction (m or μm)
R_g	radius of grain envelope (m or μm)
$R_{g,i}$	radius of growing grains in size class *i* (m or μm)
$\dot{T}$	Cooling rate (K/s)
T_l^0	liquidus temperature of the alloy (K)
$T(r)$	local temperature (K)
$T_l(r)$	local liquidus temperature (K)
T_n	critical nucleation temperature of the melt (K)
ΔT	maximum total undercooling in the melt (K)
ΔT_r	curvature undercooling (K)
ΔT_{fg}	free growth undercooling for specific inoculation particles (K)
$\Delta T(r)$	local undercooling (K)
$V_{g,i}$	growth rate of globular grain in size class *i* (m/s)
$V_{d,i}$	dendrite tip growth velocity of grain size class *i* (m/s)
Vol_{INZ-II}	volume of the INZ-II (m^3)
Vol_{domain}	volume of the whole calculation domain (m^3)

Greek symbols

Γ	Gibbs-Thomson coefficient (m K)
Ω_i	solute supersaturation ratio of grain class i
δ_{SSN}	thickness of the solute suppressed nucleation (SSN) zone (m or μm)
δ_{INZ-I}	thickness of the 'inhibited nucleation zone' (INZ) I (m or μm)
δ_c	thickness of the solute diffusion layer (m or μm)